SCK • CEN

STUDIECENTRUM VOOR KERNENERGIE
CENTRE D'ÉTUDE DE L'ÉNERGIE NUCLÉAIRE

# Fracture Toughness Derived from Small Circumferentially Cracked Bars

**Marc Scibetta and Rachid Chaouadi**

**SCK•CEN, Boeretang 200,
B-2400 Mol, Belgium.**

**November 1997**

**BLG-761**

# Fracture Toughness Derived from Small Circumferentially Cracked Bars

**Marc Scibetta and Rachid Chaouadi**

**SCK•CEN, Boeretang 200,**
**B-2400 Mol, Belgium.**

**November 1997**

**BLG-761**

Marc Scibetta[1] and Rachid Chaouadi[1]

# FRACTURE TOUGHNESS DERIVED FROM SMALL CIRCUMFERENTIALLY CRACKED BARS

---

**REFERENCE:** Scibetta, M. and Chaouadi, R., **"Fracture Toughness Derived from Small Circumferentially Cracked Bars,"** "Small Specimen Test techniques", ASTM STP 1329, W. R. Corwin, S. T. Rosinski, E. van Walle, Eds., American Society for Testing and Materials, 1997.

**ABSTRACT:** Small circumferentially Cracked Round Bars (CRB) are used to derive the fracture toughness of reactor pressure vessel steels. This cylindrical geometry is of practical interest for the nuclear industry as it only requires a small amount of irradiated material and as it is easy to test on a tensile machine.

This paper describes an experimental procedure to obtain fracture toughness measurements from CRB with a diameter of 10 mm. Emphasis is put on crack growth monitoring during rotating bending fatigue precracking, on the formulae used to analyse the load displacement trace of a fracture toughness test and on the correction to be applied to take the loss of constraint into account.

Experiments show that the method has the potential to derive fracture toughness values from the lower shelf to the lower transition region. Finite element analysis shows that the constraint of this geometry is generally lower than for bend specimens but is higher at higher load levels, allowing comparison to toughness data valid according to prevailing standards.

**KEY WORDS:** miniaturisation, circumferentially Cracked Round Bar (CRB), fracture toughness, finite element analysis, lower shelf, transition region, cleavage, precracking, rotating bending fatigue, Pre-Cracked Charpy V-notch (PCCV), A533B-Cl.1, 22NiMoCr37.

---

Testing methods to measure the fracture toughness in the lower or the upper shelf region are now well-established on a limited number of specimen geometries and are described in

[1] SCK•CEN, Boeretang 200, B-2400 Mol (Belgium)

different standards. However, to obtain valid measurements, size criteria should be verified. As a result, the specimen size to be tested is large in the lower and the transition region. For example, the recommendation of the ASTM Standard Test Method for Plane Strain Fracture Toughness of Metallic Materials (E 399-83) is:

$$B,\ a \geq 2.5 \left( \frac{K_{Ic}}{\sigma_{YS}} \right)^2 \tag{1}$$

where $B$ is the specimen thickness, $a$ the crack length , $\sigma_{YS}$ the yield strength and $K_{Ic}$ the plane-strain fracture toughness.

It was thus suggested to apply J-integral methods based on an Elastic Plastic Fracture Mechanics (EPFM) theory, already used to measure the resistance to initiation of stable crack growth in metals ($J_{Ic}$), to measure the onset of cleavage ($J_c$). The fracture toughness is related to the J-integral through $K_{Jc}$ defined as:

$$K_{Jc} = \sqrt{\frac{J_c E}{1 - \nu^2}} \tag{2}$$

where $E$ is the Young's modulus and $\nu$ the Poisson's ratio.

However, cleavage is a stress controlled fracture mechanism and is very sensitive to loss of constraint. On this basis, a size limit requirement has recently been integrated in the ASTM Standard Test Method for J-integral Characterization of Fracture Toughness (E1737-96):

$$B,\ b,\ a \geq 200 \frac{J_c}{\sigma_Y} \tag{3}$$

where $b$ is the uncracked ligament length and $\sigma_Y$ the effective yield strength calculated as the average of the yield strength $\sigma_{YS}$ and the ultimate tensile strength $\sigma_{TS}$.

Moreover, if the size limit is not satisfied, Anderson and Dodds [1] proposed a constraint correction equation, Eq 4, for the J-integral to obtain the equivalent toughness in Small Scale Yielding (SSY) condition. This equation is established for bend geometries with a crack length-to-width ratio of 0.5 ($a/W$=0.5).

$$J_{SSY} = \frac{J}{1 + \phi \left( \frac{J}{b\ \sigma_{YS}} \right)^{\gamma}} \tag{4}$$

where $\phi$ and $\gamma$ depend on the strain-hardening exponent. For example, for a strain-hardening exponent $n = 10$, $\phi = 154.2$ and $\gamma = 1.31$.

$J_{SSY}$ increases as a function of J up to a plateau that limits the $J_{SSY}$ value obtainable from a test. The derivate of Eq 4 gives the maximum $J_{SSY}$ and the size limitation:

$$\frac{\partial J_{SSY}}{\partial J} = 0 \quad \Rightarrow \quad b \geq \frac{\gamma}{1-\gamma} \left(\phi\,(\gamma-1)\right)^{\frac{1}{\gamma}} \frac{J_{SSY}}{\sigma_{YS}} = \left(\phi\,(\gamma-1)\right)^{\frac{1}{\gamma}} \frac{J}{\sigma_{YS}} \qquad (5)$$

Consequently, the largest corrected fracture toughness $K_{Jc}$ derivable from a typical Pre-Cracked Charpy V-notch (PCCV) is about 80 MPa $\sqrt{m}$ ( $b = 5$ mm, $n = 10$, $\sigma_{YS} = 450$ MPa).

In order to measure fracture toughness up to high values, the CRB is selected because the constraint of this geometry is maintained up to a higher load level. The size of the CRB is taken to be similar to the PCCV in order to allow comparison of the two geometries (see Fig. 2). However, as this geometry is not mentioned in any existing test standard, an in-depth study needs to be performed to precrack the specimen, to test it and to measure the fracture toughness.

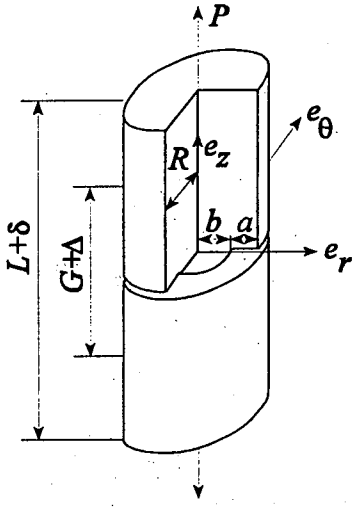


FIG. 1--Geometry of the circumferentially-cracked round bar under tensile loading. δ is the load point displacement and Δ is the gauge length displacement.

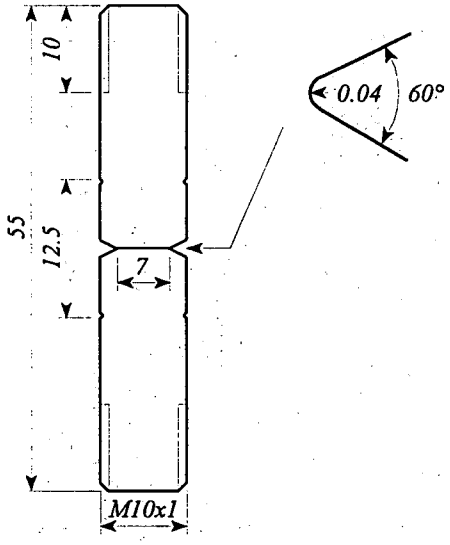


FIG. 2--Specimen size; the threads are machined after precracking the specimen.

## MATERIALS

This study is limited to two very different pressure vessel steels for which fracture toughness data on Compact Tension (CT) specimen are available in the transition region. The first is a German DIN 22NiMoCr37 steel, and is a forged, quenched and tempered steel with a high upper shelf [2]. The second is an A533 grade B class 1 steel with a low upper shelf for which data were generated in the Japan Society for the Promotion of Science (JSPS) round robin [3]. It is artificially embrittled through high phosphor and sulphur content. This material is of particular interest to simulate irradiated embrittled vessel steel.

TABLE 1--Chemical composition of the selected steels (wt%).

| | C | Si | P | S | Cr | Mn | Ni | Cu | Mo | Al |
|---|---|---|---|---|---|---|---|---|---|---|
| 22NiMoCr37 | 0.22 | 0.23 | 0.006 | 0.004 | 0.39 | 0.88 | 0.84 | 0.08 | 0.51 | ... |
| A533B-Cl.1 | 0.24 | 0.41 | 0.028 | 0.023 | 0.08 | 1.52 | 0.43 | ... | 0.49 | 0.005 |

TABLE 2--Tensile mechanical properties of the selected steels at ambient temperature. R.A. is the Reduction of Area.

| | Orientation | $\sigma_{YS}$ (MPa) | $\sigma_{TS}$ (MPa) | $\varepsilon_{TS}$ (%) | R.A.(%) |
|---|---|---|---|---|---|
| 22NiMoCr37 | L | 456 | 608 | 10 | 73 |
| A533B-Cl.1 | T | 461 | 638 | 10 | 59 |

## PRECRACKING OF CRB SPECIMENS

Before fracture toughness testing, specimens have to be precracked by fatigue. This is a delicate and time-consuming phase. Indeed, the precrack should have adequate length and should be exempt of irregularities such as eccentricity or ovalisation. Moreover, the load should not be too high in order to avoid crack blunting and a large plastic zone at the crack tip.

The rotating bending fatigue is a very suitable technique and is chosen to be implemented on conventional drilling equipment (see Fig. 3).

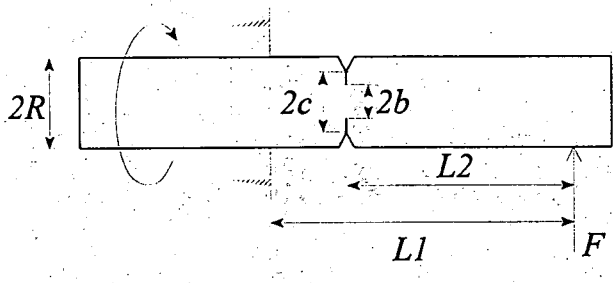


FIG. 3--Cantilever beam configuration, 2c is the ligament size after machining of the notch, 2b is the ligament size after precracking. The specimen is fixed in a collet chuck and turns at a 1000 rpm. The load, measured with a load cell, is applied through a fixed load point displacement.

However, the crack length during precracking should be evaluated in order to obtain specimens with similar crack length; this can achieved by monitoring the load decrease.

Indeed, due to crack propagation, the load is relaxed and can be correlated to the crack length. An analytical model based on the compliance of the system has been developed in order to improve the understanding of the parameter governing the correlation between the load drop and the crack length

The load drop is related to the change of compliance as:

$$1 - \frac{F_{final}}{F_{initial}} = 1 - \frac{C(\frac{c}{R})}{C(\frac{b}{R})} \tag{6}$$

where $C$ is the compliance of the total system [4]:

$$C(b/R) = C_{att.} + \frac{4\ L_1^3}{3\ E\ \pi\ R^4}[\ 1 + \frac{3.525\ R^2}{4\ L_1^2} + 24\ \pi\ \frac{1-\nu^2}{L_1^3}\ R\ L_2^2\ H(b/R)] \tag{7}$$

with

$$H(x) = \frac{0.046875}{x^3} - 0.06303639 - 0.04006494\ x^2 + 0.03450366\ x^3 + 0.009301849\ x^4 + 0.004570464\ x^5 + 0.002724667\ x^6 + 0.0001693451\ x^7 + 0.004956346\ x^8 \tag{8}$$

where $C_{att.}$ is the system attachment compliance.

To validate the developed model, several specimens are precracked up to different percentages of load decrease and then broken at liquid nitrogen temperature. Figure 5 shows the correlation between the measured crack length ratio and the load drop and confirms good agreement of the experiment with the developed model. The ligament diameter and the eccentricity is measured using a digital profile projector. The ligament diameter is obtained form the best fit circle trough 8 equally spaced points around the crack. The centre of the bar is obtained from the best fit circle trough 4 equally spaced point around the bar. The distance between the centres of the two circles is the eccentricity (see Figure 4).

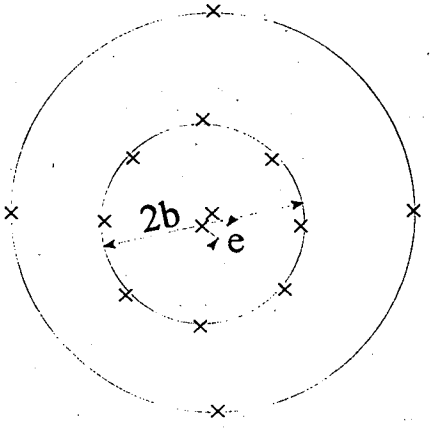


FIG. 4--Measurement of ligament length and eccentricity using digitalized coordinates. The least square method is used in order to obtained the best fit circle.

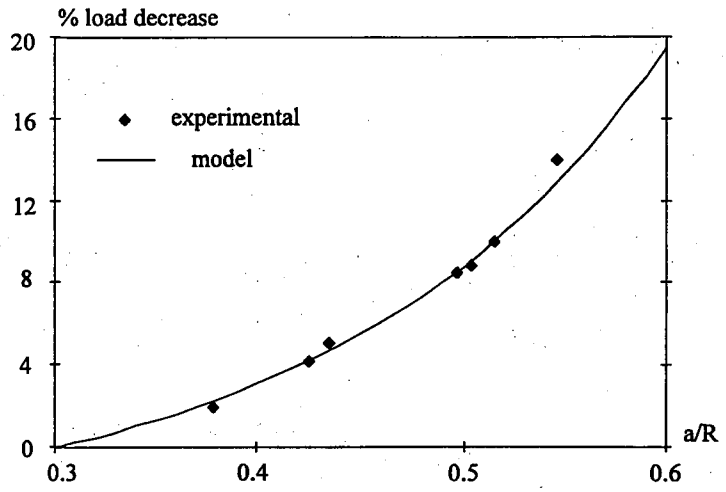


FIG. 5--A theoretical relation between the load drop and the crack length is established and experimentally confirmed using a 18MND5 French steel.

The load should be limited in order to restrict the maximum stress intensity factor to an acceptable value (in our case the limit is 20 MPa $\sqrt{m}$). This condition can be satisfied using an adapted formula for CRB under bending, namely:

$$K = S\left(\frac{b}{c}\right) G\left(\frac{b}{R}\right) \sigma \sqrt{\frac{\pi\, a\, b}{R}} \quad \text{with} \quad \sigma = \frac{4M}{\pi b^3}, \tag{9}$$

with
$$G(x) = \frac{3}{8}\left[1 + \frac{1}{2}x + \frac{3}{8}x^2 + \frac{5}{16}x^3 + \frac{35}{128}x^4 + 0.531x^5\right] \tag{10}$$

and
$$S(y) = -0.0184298 + 0.408542y + 1.05795y^2 - 0.448753y^3 \qquad y \geq 0.4 \tag{11}$$

where $M$ is the applied bending moment, $G$ is the function derived by Benthem and Koiter [5] and $S$ takes the contact of crack lips into account [4,6,7]. The model used to derive the $S$ function is based on an elastic material model.

A summary of precracking results is reported in Table 3 and typical results are shown in Figure 6. Specimens were precracked in order to obtain crack length to radius ratio of about 0.5. The eccentricity and the scatter on the crack length are both small allowing specimens to be used for fracture toughness tests.

TABLE 3--Precracking results with mean values and associate standard deviation.

| | Sample size (N) | Ligament diameter (mm) | Eccentricity (mm) | Time (min.) |
|---|---|---|---|---|
| 22NiMoCr37 | 15 | 5.02 ± 0.14 | 0.080 ± 0.036 | 59 ± 22 |
| A533B-Cl.1 | 18 | 5.04 ± 0.12 | 0.044 ± 0.023 | 47 ± 5 |

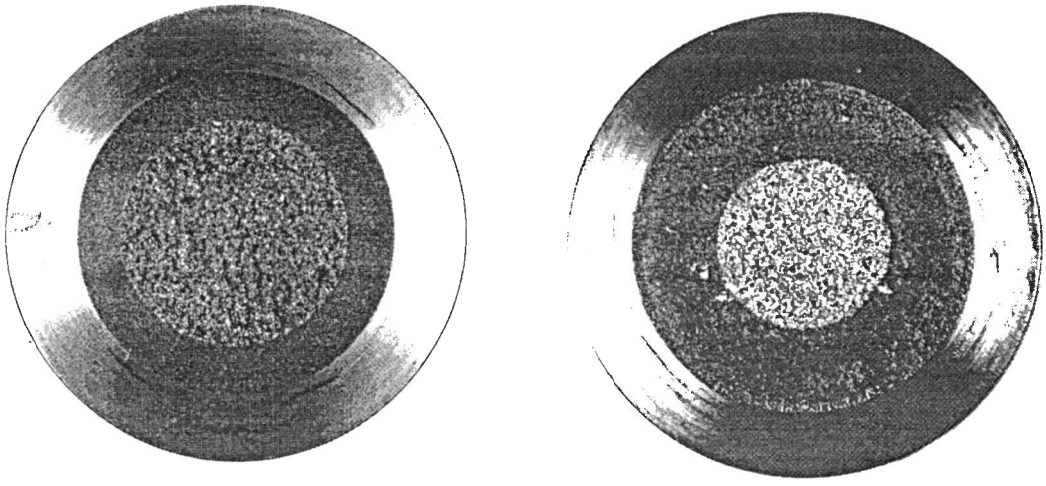

FIG. 6--Typical precracked specimen. The deep and shallow cracks are concentric.

## FRACTURE TOUGHNESS TESTING

The precracked specimens are loaded in tension in order to derive the fracture toughness value. However, as no existing standard describes a procedure to be followed, special attention was given to describe and verify the test, and to check the formulae to derive the fracture toughness.

The load displacement trace is used to obtain the J-integral at fracture as:

$$J = \frac{K^2(1-\nu^2)}{E} + \eta \frac{U_{pl.}}{\pi b^2} \quad \text{with} \quad U_{pl.} = \int_0^{\delta_{pl.}} P \, d\delta_{pl.} \tag{12}$$

where $\delta_{pl.}$ is the plastic part of the displacement and $U_{pl.}$ the plastic energy dissipated during the test.

The stress intensity factor is evaluated through Benthem and Koiter's formula [5] as this formula is closer to the finite element solution (2% difference)[4] than functions proposed by other authors [8,9]:

$$K = G(\frac{b}{R}) \frac{P}{\pi b^2} \sqrt{\frac{\pi a b}{R}} \tag{13}$$

with

$$G(x) = \frac{1}{2} [1 + \frac{1}{2}x + \frac{3}{8}x^2 - 0.363x^3 + 0.731x^4] \tag{14}$$

where $P$ is the tensile load, $a$ the crack length, $2b$ the ligament diameter and $2R$ the bar

diameter (Fig.1).

Finite element calculations [10] showed that the following proposed equation has a mean accuracy of 5% in the range of interest:

$$\eta = 1 - \frac{1.0875 \left( 1.155 - 2.06 \frac{a}{R} + 1.13 \left(\frac{a}{R}\right)^2 \right)}{1 + 0.007 \frac{b}{\delta_{pl.}}} \tag{15}$$

The load point displacement is measured using the average value of the gage displacement as obtained from two extensometers mounted in opposition.

$$\delta = \frac{\Delta_1 + \Delta_2}{2} \tag{16}$$

The plastic part of the displacement is evaluated using:

$$\delta_{pl.} = \Delta - C_G P \tag{17}$$

here $C_G$ is the slope of the load displacement curve in the linear elastic region. This slope is experimentally measured from linear regression, taking only points for which the load is less than 33.3% of the maximum load. The level of 33.3% is chosen in order to remain in the linear elastic region and to have a sufficient range to obtain an accurate linear regression.

It is then possible to evaluate the fracture toughness from the load displacement trace using the former equation. However, it is advisable to verify the test results by comparing:

1) The difference between the two extensometers displacement at rupture because it is an indication of an existing bending moment at rupture due to misalignment or eccentricity. It can also be due to measurement accuracy as displacement to be measured are largely smaller than for bend geometries. Tests were considered to be valid when:

$$\| \Delta_1^{end} - \Delta_2^{end} \| \leq 0.3 \ \delta^{end} \tag{18}$$

2) The experimental specimen compliance $C_G$, to the theoretical value derived from the Benthem and Koiter stress intensity function.

$$C_G^{th.} = \frac{\Delta}{P} = \frac{G}{E \pi R^2} \left( 1 + 4 \pi \frac{1 - \nu^2}{G} R H\left(\frac{b}{R}\right) \right) \tag{19}$$

with
$$H(x) = \frac{0.25}{x} - 0.3531717 + 0.168875 x^2 - 0.1325521 x^3 + 0.04880469 x^4 - 0.01106345 x^5 + 0.05044688 x^6 - 0.03803811 x^7 + 0.01669878 x^8 \tag{20}$$

Tests are considered to be valid when the difference is less than 15%:

$$\| C_G^{th.} - C_G \| \leq 0.15 \ C_G^{th.} \tag{21}$$

It should be noted that in the context of the establishment of a standard test method, the theoretical compliance $C^{th}{}_G$ might be used instead of the measured compliance $C_G$ in Eq 17.

## FINITE ELEMENT CALCULATIONS AS A SUPPORT TO THE UNDERSTANDING OF LOSS OF CONSTRAINT

Fracture toughness tests are intended to characterise the plane strain fracture toughness. To keep the crack tip under plane strain conditions, the specimen should be sufficiently large. In order to compare very large specimens to small ones, the Small Scale Yielding (SSY) solution is introduced. This SSY condition requires a very small plastic zone relative to the size of the specimen. The deviation from this SSY crack tip condition characterises the loss of constraint of the specimen. Although the loss of constraint results in an apparent higher fracture toughness, loss of constraint cannot be easily measured experimentally but can be determined through finite element analysis. A commonly adopted measure of this constraint loss is the Q-factor that is defined as the difference between the opening stress at a typical distance from the crack tip and the SSY condition:

$$Q = \left. \frac{\sigma_{\theta\theta} - \sigma_{\theta\theta}^{SSY}}{\sigma_{YS}} \right|_{at\ r = 2J/\sigma_{YS}} \tag{22}$$

where r is the distance from the crack tip. This Q factor is considered to be a unique factor characterizing the stress field if Q is independent of the r distance and if the stress contours are self-similar [12].

The Q-factor is zero for low load levels and decreases as the load increases due to the loss of constraint. To compare the loss of constraint of the CRB with edge crack bend specimens, the two geometries are analysed using finite element calculation.

The incremental theory of plasticity is used in combination with an isotropic strain-hardening model based on the Von Mises criterion with a true stress-strain curve described by a power law:

$$\frac{\sigma}{\sigma_{YS}} = \begin{cases} \dfrac{\varepsilon}{\varepsilon_{YS}} & if \quad \sigma < \sigma_{YS} \\ \left(\dfrac{\varepsilon}{\varepsilon_{YS}}\right)^{1/n} & if \quad \sigma \geq \sigma_{YS} \end{cases} \tag{23}$$

with

$$E\ \varepsilon_{YS} = \sigma_{YS} \tag{24}$$

The study is limited to one material with a strain-hardening exponent of $n = 10$ and a ratio of yield stress to Young's modulus of $E/\sigma_{YS} = 500$. Each mesh contains about 250 eight-node 2D axisymetric elements with reduced Gauss integration. Because of large geometry changes, the updated Lagrangian procedure is used to account for large strains and

displacements. To avoid large mesh deformation and overlapping at the crack tip, an initial blunted mesh is used. The initial crack tip radius is chosen such that the Crack Tip Opening Displacement (CTOD) is five times larger than its initial value (see Fig. 7). The smallest element located at the crack tip has as a typical dimension of the crack tip initial radius divided by five. The mesh size and density are chosen to reduce computer time and to keep the solution nearly insensitive to mesh size. The load is simulated by a vertical displacement of nodes situated at the outer face.

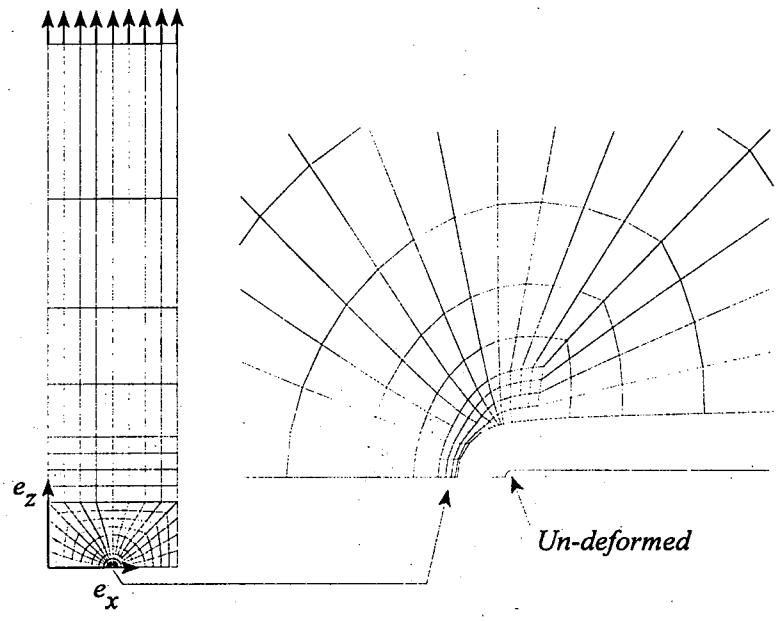


FIG. 7--Deformed mesh due to a tensile load. The mesh density at the crack tip is chosen to avoid large mesh distortion.

Different analyses are performed with varying initial CTOD (from 0.25 to 64 μm) to cover small to large scale yielding. Q-factor results are found to be independent of the initial CTOD as long as the final CTOD is larger than 3 times the initial one and the final deformed crack tip mesh is not overlapped. Moreover too large mesh distortion can induce a loss of convergence of the solver. The independence of Q-factor as a function of the scaled distance from the crack tip is verified using the quantity:

$$Q' = \|Q(2) - Q(5)\| \tag{25}$$

$Q'$ is less than 0.05 up to $J/a\sigma_{YS}$=0.04 and less than 0.1 up to $J/a\sigma_{YS}$=0.13.
The self-similarity of the maximal principal stress contours is verified up to $J/a\sigma_{YS}$=0.13 and is shown in Figure 8.

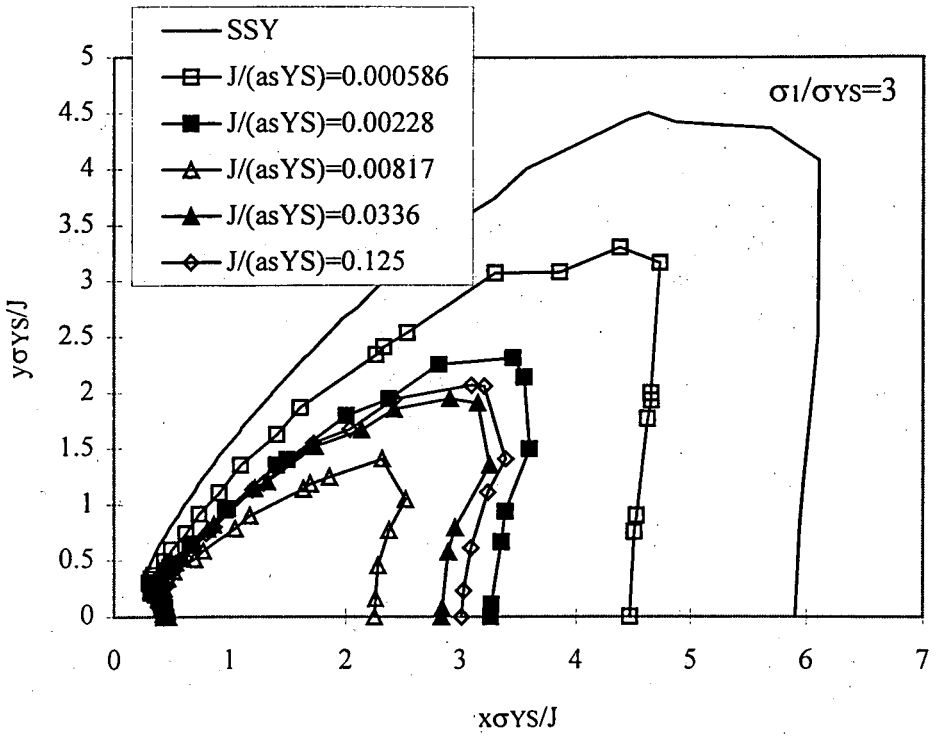


FIG. 8--Maximal principal stress contour ahead of the crack tip for different load levels.

Figure 9 shows the Q-factor, as defined by Eq 4, as a function of the load level expressed by $J/(a\sigma_{YS})$. The reference small scale yielding value used to calculate the Q-factor is obtained by applying the far displacement linear elastic field as boundary condition of a circular region containing an edge crack. The opening stress calculated at a distance of $r\sigma_{YS}/J=2$ is $\sigma^{SSY}/\sigma_{YS} = 3.46$. Figure 9 shows that constraint loss of bend specimens begins at load higher than the requirement of Eq 3 (E1737 $J_c$). For the CRB specimen, the constraint decreases initially at low loads but is maintained high at higher load levels. This theoretical result, also reported by Giovanola [11], shows the potentiality of small CRB specimens to derive high fracture toughness values.

The analysis shows that at $J/(a\sigma_{YS}) = 0.0044$, the plastic zone crosses the $e_z$ axis. At this load level the constraint is nearly the lowest, while, the load displacement trace is nearly linear (5.1 % offset). This result clearly shows that a linear load displacement trace does not mean a dominant elastic condition at the crack tip and data obtained in this linear domain should be used cautiously.

For $J/(a\sigma_{YS}) = 0.077$, the ligament is fully plastic but confined to the ligament. This confinement seems to be the reason for an increase of the Q-factor.

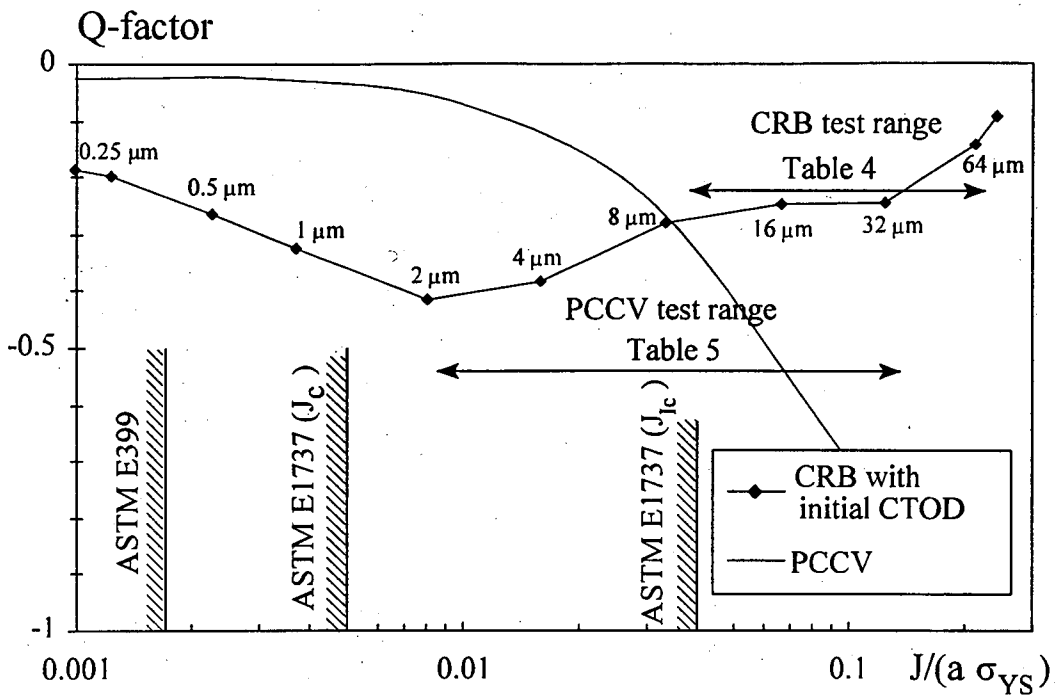


FIG. 9--The Q-factor as a function of the J-integral. Initial CTOD used in finite element analyses is indicated in µm. The edge crack bend results are obtained using 2 dimensional plane strain analyses[12].

## RESULTS AND DISCUSSION

Tests were performed on a 100kN INSTRON tensile machine under controlled displacement at a constant crosshead speed of 0.2mm/min. The specimen together with the grips are cooled with liquid nitrogen vapour in an environmental chamber. The specimen temperature is maintained constant within +-2°C during 30 min prior to and during the test. Elongation of the specimen is measured by two extensometers mounted in opposition with an initial gauge length of 12.5mm. This special mounting of the extensometers allows the evaluation of eventual bending due to misalignment or eccentricity. A four-channel data acquisition system equipped with a recorder allows the logging of load, displacement of the two extensometers and the cross head displacement.

Equation 12 to 21 are now applied to analyse the load displacement traces of 33 tests. The output of this analysis is summarized in Table 4.

Pre-Cracked Charpy V-notch (PCCV) specimens are also tested in order to obtain direct comparison with the CRB. The results are summarised in Table 5.

TABLE 4--Summary of performed tests on 10 mm CRB. The results of the tests are given with their mean value and their associated standard deviation. All tests are valid according to Eq 18 and 21 except the tests at -154°C. The fixture of the clip gauge at -154°C is believed to be the cause of the discrepancy at this temperature.

| Material | Temp. (°C) | Sample size (N) | $\frac{\|C_G^{th.} - C_G\|}{C_G^{th.}}$ (%) | $\frac{\|\Delta_1^{end} - \Delta_2^{end}\|}{\delta^{end}}$ (%) | $J_c$ (N/mm) | $K_J$ (MPa $\sqrt{m}$) |
|---|---|---|---|---|---|---|
| A533B-Cl.1 | 25 | 6 | 1.5 ± 1.2 | 8.5 ± 3.2 | 107 ± 14 | 155 ± 10 |
| A533B-Cl.1 | 0 | 6 | 0.9 ± 0.7 | 8.9 ± 10.3 | 73 ± 36 | 126 ± 29 |
| A533B-Cl.1 | -25 | 6 | 2.5 ± 2.1 | 9 ± 7.5 | 48 ± 10 | 104 ± 10 |
| 22NiMoCr37 | -60 | 6 | 5.6 ± 4.6 | 10.6 ± 8 | 271 ± 90 | 243 ± 49 |
| 22NiMoCr37 | -91 | 6 | 6.7 ± 5.3 | 9.5 ± 10 | 130 ± 64 | 167 ± 41 |
| 22NiMoCr37 | -154 | 3 | 42.5 ± 43.5 | not available | 26 ± 10[†] | 75 ± 16[†] |

[†] Values recalculated with theoretical compliance are: $J_c$=31±8 and $K_J$=84±11

TABLE 5--Summary of performed tests on PCCV specimens. Specimens from A533B-Cl.1 and 22NiMoCr37 material are respectively 20% and 0% side grooved. Results of tests are given with their mean value and their associated standard deviation.

| Material | Orientation | Temp. (°C) | Sample size (N) | $J_c$ (N/mm) | $K_J$ (MPa $\sqrt{m}$) |
|---|---|---|---|---|---|
| A533B-Cl.1 | T-L | 25 | 4 | 198 ± 34 | 211 ± 18 |
| A533B-Cl.1 | T-L | 0 | 10 | 92 ± 31 | 143 ± 23 |
| A533B-Cl.1 | T-L | -25 | 6 | 42 ± 21 | 95 ± 25 |
| 22NiMoCr37 | L-S | -60 | 6 | 383 ± 95 | 295 ± 38 |
| 22NiMoCr37 | L-S | -91 | 6 | 107 ± 78 | 148 ± 59 |
| 22NiMoCr37 | L-S | -154 | 3 | 14 ± 5 | 55 ± 12 |

After optical crack length measurement, the specimens with the highest fracture toughness value were analysed with a Scanning Electron Microscope (SEM) in order to point out eventual ductile crack extension. However, for both materials, no ductile crack growth evidence was found. Although all specimens failed by cleavage, no single cleavage initiator was found. Many specimens from A533B-Cl.1 material showed large inclusions oriented in

the rolling direction (L) demonstrating the anisotropy of this material.

The generated fracture toughness data are now compared to the results obtained in the JSPS Round Robin [3] . Figure 10 clearly shows that small specimens tend to over estimate the fracture toughness.

As the specimens are tested within the ductile to brittle transition region the statistical thickness correction proposed by Wallin [13] is applied:

$$K_{1T} = (K_{spec.} - 20)\left(\frac{B_{spec.}}{B_{1T}}\right)^{1/4} + 20 \qquad (K \text{ in MPa}\sqrt{\text{m}}) \tag{26}$$

where $B_{spec.}$ is the crack length.

Figure 11 shows that the fracture toughness scaled to 1 inch thickness is relatively independent of the specimen size. However, for both materials, PCCV and CRB specimens show an over-estimation of the scaled fracture toughness. This discrepancy is smaller for the CRB than for PCCV, particularly at high test temperatures. This indicates that the main cause of fracture toughness over-estimation is the loss of constraint.

Therefore, the constraint correction equation (Eq 4) is applied (see Fig. 12) to all PCCV and Compact Tension CT bend specimens ($n$ = 10). However this constraint correction equation was not developed for the CRB.

As shown in Fig. 9, the constraint of CRB does not decrease as a function of load but is quite constant ($Q$=-0.25 in the tested region). This constraint loss of -0.25 corresponds for a bend specimen to $J/(a\sigma_{YS}) = 0.03$ and to a constraint correction of:

$$J_{SSY} = \frac{J}{2.56} \tag{27}$$

As Q-factor is nearly independent of the scaled distance and as the stress contour are self-similar, we can assume that the constraint correction is uniquely related to the Q-factor, Eq 27 is thus applied to the CRB in Fig. 12. Moreover, preliminary results obtained using the approached proposed by Anderson and Dodds [1], give a ratio $J/J_{SSY}$= 2.1.

Figure 12 shows that the applied correction tends to improve the quality of results for CRB and PCCV. However, for PCCV at 25°C, the correction cannot be applied because the limiting 80 MPa $\sqrt{\text{m}}$ is reached. It should also be noted that the bend specimen correction (Eq 4) tends to reduce the scatter through the drastic correction for very high values.

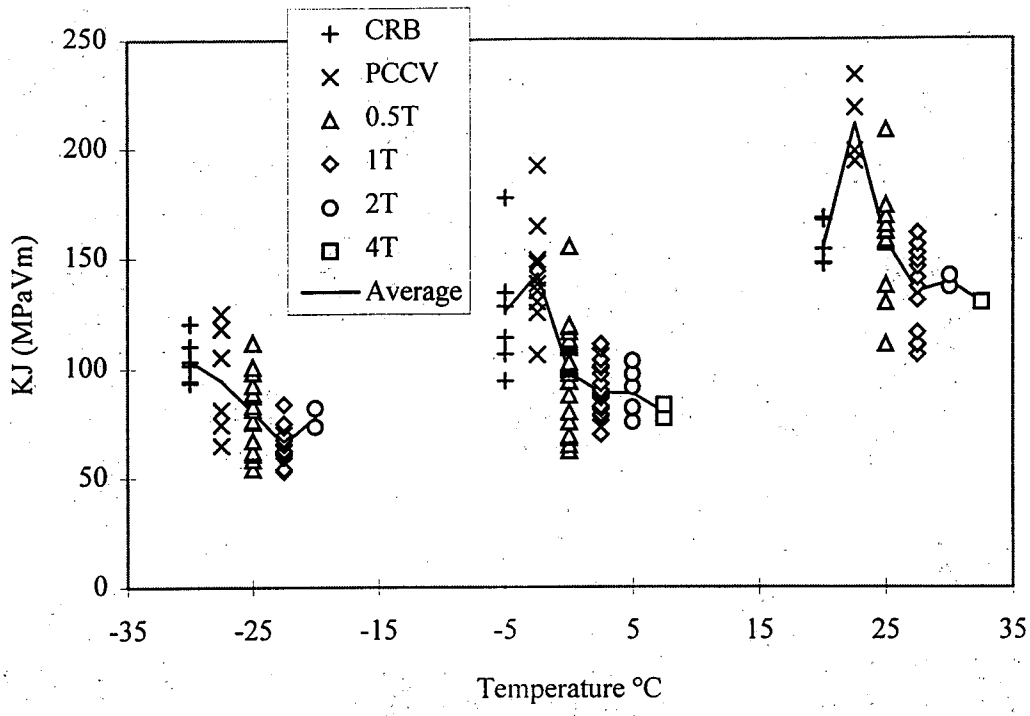


FIG. 10--Comparison to compact tension specimen (0.5 to 4 inch thickness) for the A533B-Cl.1 material. No size or constraint correction is taken into account.

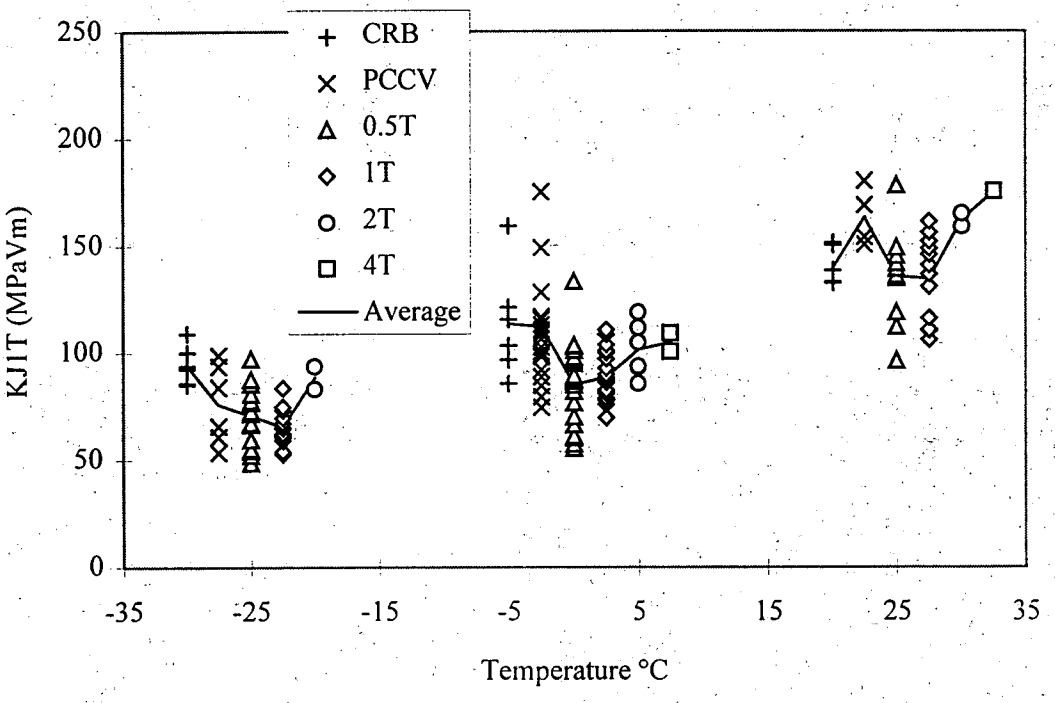


FIG. 11--Comparison to compact tension specimen (0.5 to 4 inch thickness) for the A533B-Cl.1 material. All data are scaled to 1 inch (25.4 mm) thickness in order to correct for statistical size correction. CRB are corrected according to the crack front length.

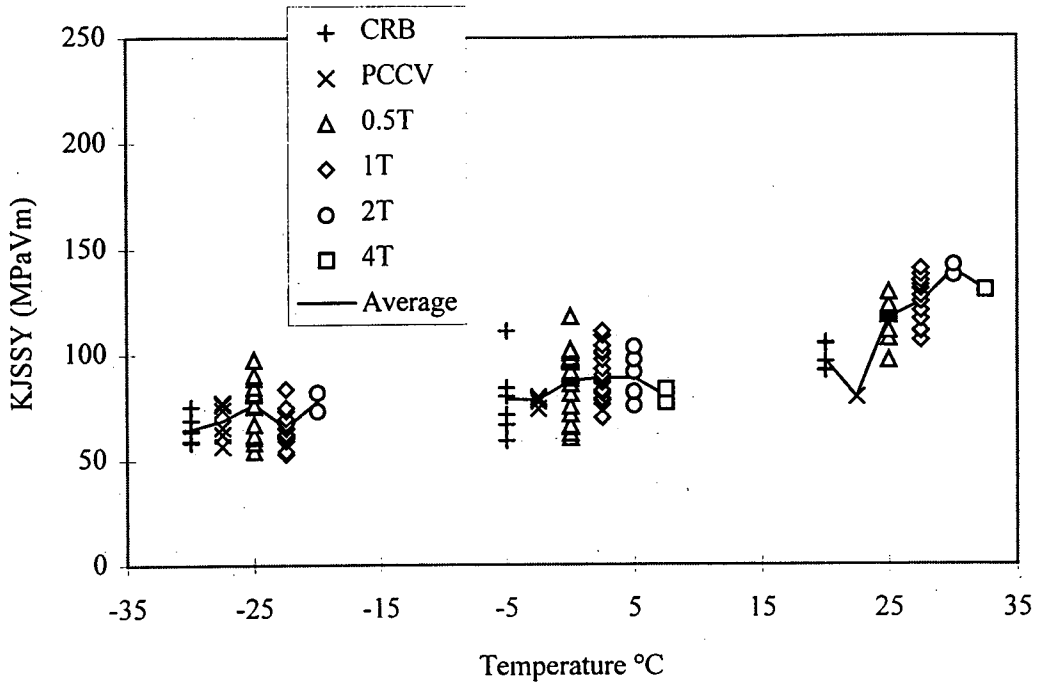


FIG. 12--Data correction for loss of constraint (Eq 4 for PCCV and CT and Eq 27 for CRB) applied to A533B-Cl.1 material. No size correction is taken into account.

## CONCLUSIONS

The precracking of the circumferentially notched bar specimen can be achieved successfully using the rotating bending fatigue technique. It results in excellent accuracy in crack length determination by applying an analytical model and negligible eccentricity of the ligament within an acceptable time.

Fracture toughness tests with CRB should be performed carefully to avoid unreliable results. Two important checks are recommended, namely: the comparison between the linear elastic compliance of the specimen and the theoretical analytical formula; and the elongation of the specimen through two extensometers mounted in opposition.

The evaluation of the Q-factor for the CRB shows that the constraint decreases initially but is maintained high at higher load levels and is higher than for bend specimens.

Test results show that the CRB over-estimates (2.5 higher values) the fracture toughness in the region of interest due to loss of constraint. However, the over-estimation is less than for the PCCV. Moreover, it is possible to apply some correction factors to take constraint loss into account.

## ACKNOWLEDGEMENTS

The authors would like to express their gratitude to K. Onizawa for his contribution to experimental testing, E. van Walle and Prof. Nguyen-Dang Hung for reviewing the paper and to R. Mertens, R. Sneyers, L. Van Houdt, A. Verstrepen and J.P. Wannijn for their technical assistance. This work is financially supported by Tractebel Energy Engineering whose permanent encouragement is greatly acknowledged.

## REFERENCES

[1] Anderson, T. L. and Dodds, R. H., Jr., "Simple Constraint Corrections for Subsize Fracture Toughness Specimens," Small Specimen Test Techniques Applied to Nuclear Reactor Vessel Thermal Annealing and Plant Life Extension, ASTM STP 1204, W. R. Corwin, F. M. Haggag, and W. L. Server, Eds., American Society for Testing and Materials, Philadelphia, 1993, pp. 93-105.

[2] Mudry, F. and Di Fant, M., "A round robin on the measurement of local criteria," IRSID report, No. RE 93.319, October 1993

[3] "Standard Test Method for Fracture Toughness within Ductile-Brittle Transition," in Standard of the 129th Committee, Japan Society for the Promotion of Science, 1995(in Japanese).

[4] Scibetta, M., "Precracking of Round Notched Bars", report BLG-708, pp. 1-35, SCK•CEN Mol, Belgium, February 1996.

[5] Benthem, J. P. and Koiter, W. T., "Asymptotic Approximations to Crack Problems," in Methods of Analysis and Solutions of Crack Problems (Edited by G. C. Shi), Chapter 3, Noordhoft International Publishing, Groningen, 1973, pp. 131-178.

[6] Sawaki, Y., Aoyama, N., Abe, Y., Ohshima, T. and Kawasaki, T., "Determination of Fatigue Fracture Toughness by Conventional Rotary Bending Specimen", Joint Conference on Experimental Mechanics, Oahu-Maui, Hawaii, 22-23 May 1982, pp. 555-560.

[7] Meguid, S.A., "Three-Dimensional Finite Element Analysis of Circumferentialy-Cracked Notched and Un-Notched Cylindrical Components", Engineering Fracture Mechanics, Vol. 37, No. 2, pp. 361-371, 1990.

[8] Bueckner, H. C., "Discussion on Stress Analysis of Cracks," ASTM STP 381, P. C. Paris and G. C. Shih, 1965, pp. 82-83.

[9] Haris, D. O., "Stress Intensity Factors for Hollow Circumferentially Notched Round Bars," J. of Basic Engineering., 89, 1967, pp 49-54.

[10] Scibetta, M., "Fracture Toughness Evaluation of Circumferentially-Cracked Round Bars," to be published.

[11] Giovanola, J. H., Homma, H., Lichtenberger, M., Crocker, J. E., and Klopp, R. W., "Fracture Toughness Measurements Using Small Cracked Round Bars," Constraint Effects in Fracture: Theory and Applications, ASTM STP 1244, Mark Kirk and Ad. Bakker Eds., American Society for Testing and Materials, Philadelphia, 1994.

[12] O'Dowd, N. P. and Shih, C. F., "Family of Crack-Tip Fields Characterized by a Triaxiality Parameter-I," J. of Mech. & Phys. of Solids, Vol. 39, 1991, pp. 898-1015.

[13] Wallin K., "The size effect in $K_{IC}$ results", Engineering Fracture Mechanics, Vol. 22, No. 1, pp. 149-163, 1985

## APPENDIX : FRACTURE TOUGHNESS DATA

TABLE A1-- A533B-Cl.1 with CRB.

| Spec. Id. | Temp. (°C) | 2b (mm) | Jc ($kJ/m^2$) | Kc (MPa$\sqrt{m}$) |
|---|---|---|---|---|
| 3-1-1 | 25 | 4.99 | 124 | 167.1 |
| 3-1-2 | 25 | 5 | 125.5 | 168.2 |
| 3-1-3 | 25 | 4.95 | 96.8 | 147.7 |
| 3-1-4 | 25 | 4.8 | 96.3 | 147.3 |
| 3-1-5 | 25 | 4.86 | 105.1 | 153.9 |
| 3-1-6 | 25 | 4.92 | 96.1 | 147.2 |
| 3-1-7 | 0 | 5.1 | 57.6 | 114.0 |
| 3-1-9 | 0 | 5.09 | 139.5 | 177.3 |
| 3-1-10 | 0 | 5.01 | 50.3 | 106.4 |
| 3-1-11 | 0 | 5.19 | 39.4 | 94.2 |
| 3-1-12 | 0 | 5.09 | 72.6 | 127.9 |
| 3-1-13 | 0 | 5.19 | 80.2 | 134.4 |
| 3-1-14 | -25 | 5.16 | 47.2 | 103.2 |
| 3-1-15 | -25 | 4.93 | 64.3 | 120.4 |
| 3-1-16 | -25 | 4.9 | 38.8 | 93.5 |
| 3-1-17 | -25 | 5.08 | 45.9 | 101.6 |
| 3-1-18 | -25 | 5.2 | 39.3 | 94.1 |
| 3-1-19 | -25 | 4.95 | 54 | 110.3 |

TABLE A2--22NiCrMo37 with CRB.

| Spec. Id. | Temp. (°C) | 2b (mm) | Jc ($kJ/m^2$) | Kc (MPa$\sqrt{m}$) |
|---|---|---|---|---|
| 30X1 | -60 | 5.02 | 306.5 | 266.0 |
| 30X2 | -60 | 5.18 | 296.7 | 261.7 |
| 30X3 | -60 | 5.07 | 91.5 | 145.3 |
| 30X4 | -60 | 4.78 | 312.2 | 268.4 |
| 30X5 | -60 | 4.95 | 338.8 | 279.6 |
| 30X6 | -60 | 4.88 | 281.3 | 254.8 |
| 30X8 | -91 | 5.19 | 116 | 163.6 |
| 30X9 | -91 | 5.04 | 110.8 | 159.9 |
| 30X10 | -91 | 4.89 | 59.7 | 117.4 |
| 30X11 | -91 | 4.96 | 240.2 | 235.4 |
| 30X12 | -91 | 5.04 | 90.1 | 144.2 |
| 30X13 | -91 | 5.31 | 166.6 | 196.1 |
| 30X14 | -154 | 4.96 | 35.7 | 90.8 |
| 30X15 | -154 | 5.05 | 15.1 | 59.0 |
| 30X16 | -154 | 5.25 | 26.8 | 78.6 |

TABLE A3-- 22NiCrMo37 with PCCV.

| Spec. Id. | Temp. (°C) | a (mm) | Jc ($kJ/m^2$) | Kc (MPa$\sqrt{m}$) |
|---|---|---|---|---|
| 30Y3 | -60 | 4.85 | 448.6 | 321.7 |
| 30Y4 | -60 | 5.04 | 402.8 | 304.9 |
| 30Y5 | -60 | 4.94 | 232.5 | 231.6 |
| 30Y6 | -60 | 4.89 | 390.6 | 300.2 |
| 30Y7 | -60 | 4.85 | 323.9 | 273.4 |
| 30Y22 | -60 | 4.97 | 502.2 | 340.4 |
| 30Y8 | -91 | 4.80 | 238.2 | 234.5 |
| 30Y11 | -91 | 4.81 | 81.1 | 136.8 |
| 30Y12 | -91 | 4.74 | 110.2 | 159.5 |
| 30Y14 | -91 | 4.83 | 50.0 | 107.5 |
| 30Y15 | -91 | 4.92 | 19.1 | 66.4 |
| 30Y16 | -91 | 4.89 | 143.0 | 181.7 |
| 30Y18 | -154 | 4.82 | 17.4 | 63.3 |
| 30Y19 | -154 | 4.95 | 7.3 | 41.0 |
| 30Y20 | -154 | 4.85 | 16.0 | 60.8 |

TABLE A4-- A533B-Cl.1 with PCCV.

| Spec. Id. | Temp. (°C) | a (mm) | Jc ($kJ/m^2$) | Kc (MPa$\sqrt{m}$) |
|---|---|---|---|---|
| 3-2-1 | 25 | 5.34 | 210.7 | 218.4 |
| 3-2-2 | 25 | 5.39 | 240.5 | 233.3 |
| 3-2-10 | 25 | 5.50 | 166.3 | 194.0 |
| 3-2-11 | 25 | 5.46 | 174.4 | 198.7 |
| 3-2-12 | 0 | 5.50 | 69.3 | 125.3 |
| 3-2-13 | 0 | 5.45 | 84.3 | 138.1 |
| 3-2-15 | 0 | 5.40 | 119.3 | 164.3 |
| 3-2-16 | 0 | 5.51 | 49.7 | 106.1 |
| 3-2-17 | 0 | 5.54 | 162.8 | 192.0 |
| 3-2-18 | 0 | 5.37 | 80.6 | 135.1 |
| 3-2-19 | 0 | 5.50 | 95.8 | 147.2 |
| 3-2-20 | 0 | 5.50 | 74.7 | 130.0 |
| 3-2-21 | 0 | 5.47 | 98.0 | 149.0 |
| 3-2-22 | 0 | 5.49 | 87.6 | 140.8 |
| 3-2-3 | -25 | 5.46 | 68.9 | 124.9 |
| 3-2-4 | -25 | 5.36 | 18.5 | 64.8 |
| 3-2-5 | -25 | 5.61 | 61.5 | 118.0 |
| 3-2-6 | -25 | 5.51 | 29.1 | 81.1 |
| 3-2-7 | -25 | 5.52 | 24.5 | 74.4 |
| 3-2-8 | -25 | 5.43 | 49.0 | 105.3 |